Electronic Supplementary Information for

Functional B@*m*CN-assisted photocatalytic oxidation of biomass-derived pentoses and hexoses to lactic acid

Jiliang Ma,[1,2]* Yancong Li,[1] Dongnv Jin,[1] Zulfiqar Ali,[1] Gaojie Jiao,[1] Junqiang Zhang,[1] Shuo Wang,[1] Runcang Sun [1]*

[1] Center for Lignocellulosic Chemistry and Biomaterials, College of Light Industry and Chemical Engineering, Dalian Polytechnic University, Dalian, China, 116034

[2] State Key Laboratory of Biobased Material and Green Papermaking, Qilu University of Technology, Shandong Academy of Sciences, Jinan, 250353

*Corresponding authors' E-mail: jlma@dlpu.edu.cn (Jiliang Ma) and rcsun3@dlpu.edu.cn (Runcang Sun), Tel.: +86-0411-86323652; Fax: +86-0411-86323652

1. Experimental

1.1 Materials:

Melamine ($C_3N_3H_3$, 99%), boric acid (H_3BO_3, 99%), glucose ($C_6H_{12}O_6$, 96%), xylose ($C_5H_{10}O_5$, ≥ 99%), fructose ($C_6H_{12}O_6$, 99%), mannose ($C_6H_{12}O_6$, 99%), rhamnose monohydrate ($C_6H_{12}O_5 \cdot H_2O$, 99%), arabinose ($C_5H_{10}O_5$, 98%), *p*-benzoquinone ($C_6H_4O_2$, 98%), ethylenediaminetetraacetic acid ($C_{10}H_{16}N_2O_8$, 99.5%), isopropyl alcohol (C_3H_8O, ≥ 99.9%) and tryptophan ($C_{11}H_{12}N_2O_2$, 98%) were purchased from Aladdin Chemistry Co. (Shanghai, China). Acetic acid ($C_2H_4O_2$, 99.5%), potassium hydroxide (KOH, 95%), formic acid (CH_2O_2, 99%) and 2-hydroxypropionic acid ($C_3H_6O_3$, 85%) and other reagents were obtained from Sigma-Aldrich Chemical Reagent Co., Ltd (Shanghai, China). All chemicals were directly used without further purification.

1.2 Activity tests:

To investigate the stability and cyclability of B@*m*CN-3, a series of reactions were performed under the above optimum reaction conditions. Typically, 100 mg of glucose and 30 mg of B@*m*CN-3 were added into a 15 mL pressure bottle with 10 mL of KOH solution (2 M). The reaction system was firstly stirred at dark conditions for 30 min. Afterwards, the system was conducted at 60 ^oC for 90 min under the irradiation of visible-light. In all cases, the catalysts were recovered by centrifuging for 5 min (8,000 rpm). The solid samples were washed with distilled water for several times until the filtrate became neutral. The washed catalysts were dried overnight at 80 ^oC prior to reuse. Similarly, the conversion of glucose and yield of lactic acid were analyzed by HPLC.

1.3 Characterization:

The studies of microstructure and morphology by scanning electron microscopy (SEM) and transmission electron microscopy (TEM) were conducted on Hitachis-4800 SEM and JEM-2100 CXII TEM, respectively. The atomic force microscopy (AFM) was obtained on a Nanoscope III AFM. Fourier infrared (FT-IR) spectra of catalysts were examined by a Bruker Tensor 27 spectrophotometer in the range of 400-4000 cm^{-1}, and a KBr disk containing 1% (w/w) finely ground sample was used for measurement. X-ray diffraction (XRD) patterns of the samples were performed by a

Bruker D8 Focus diffractometer. N_2 adsorption-desorption isotherm measurements were collected using a physisorption analyzer, and the Brunauer-Emmett-Teller (BET) method was used to calculate the specific surface area, as well as the desorption branch of isotherm in line with the Barrett-Joyner-Halenda method was utilized to evaluate the average pore diameter and pore size distribution of each sample. X-ray photoelectron spectroscopy (XPS) was examined by a Kratos Axis Ultra DLD spectrometer equipped with a monochromatic A1KR X-ray source. The ultraviolet-visible diffuse reflectance spectra (UV-vis DRS) of samples were recorded on a Cary 5000 spectrophotometer fitted with an integrating sphere attachment from 300 to 800 nm, and the $BaSO_4$ was used as the reference. Electro spin-resonance (ESR) spectra of all samples were detected by a JES-FA200 spectrometer. Inductively coupled plasma atomic emission spectroscopy (ICP-MS) was performed on Agilent 7800 equipment. Elemental analysis (EA) was conducted on an elemental analyzer (Elemantar Vario EL cube).

1. Results and discussion

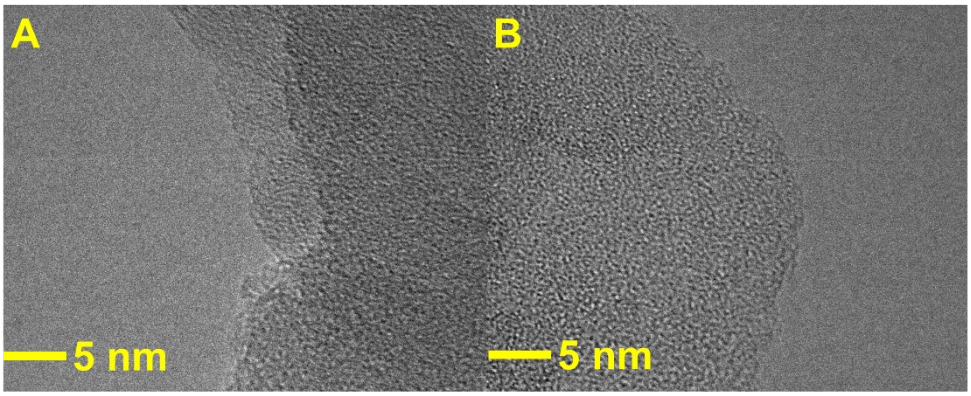

Fig. S1 HRTEM images of *m*CN (A) and B@*m*CN-3 (B).

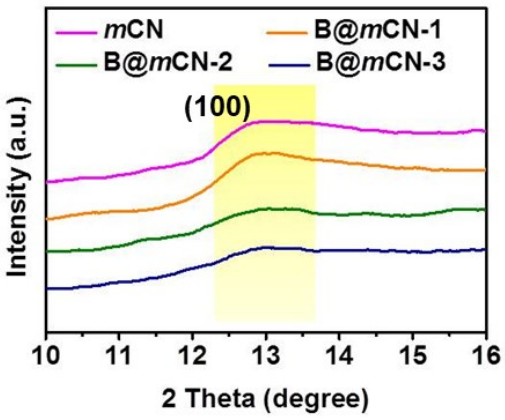

Fig. S2 XRD patterns of *m*CN and B@*m*CN.

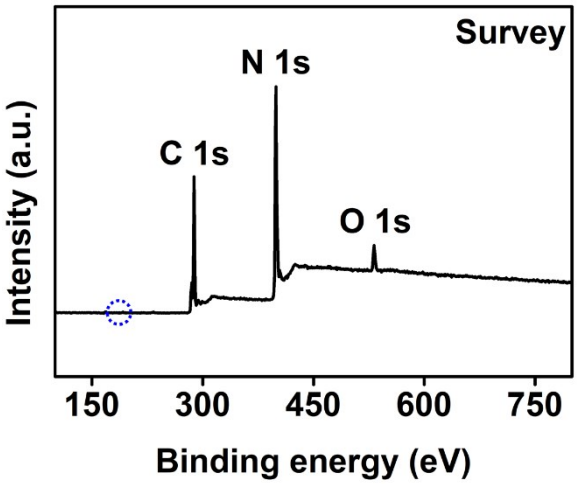

Fig. S3 XPS survey spectra of B@*m*CN-3.

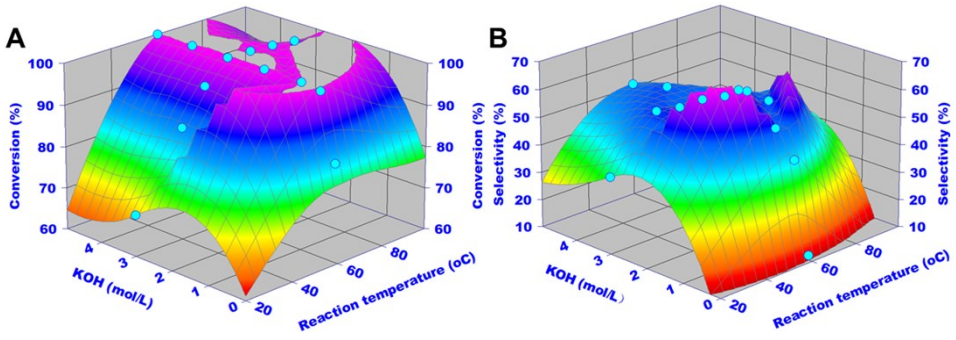

Fig. S4 The effects of KOH concentration and reaction temperatures on the conversion of glucose (A) and the selectivity of lactic acid (B).

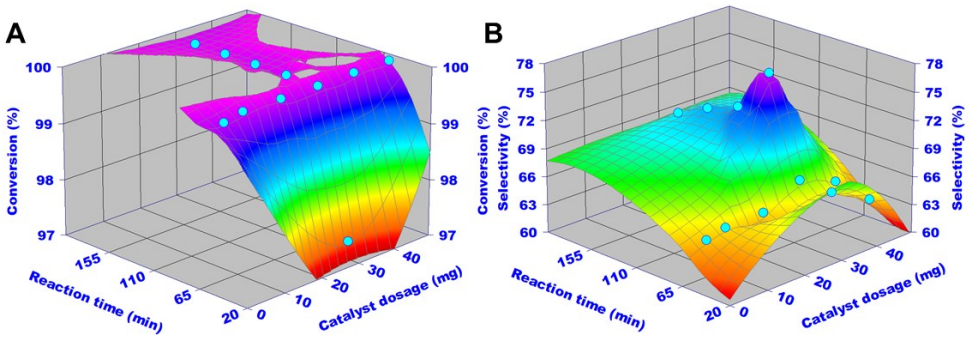

Fig. S5 The effects of reaction time and catalyst dosages on the conversion of glucose (A) and the selectivity of lactic acid (B).

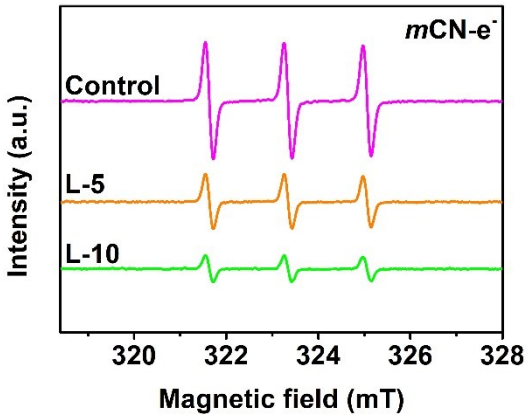

Fig. S6 TEMPO ESR spin-labelling for e^- of *m*CN.

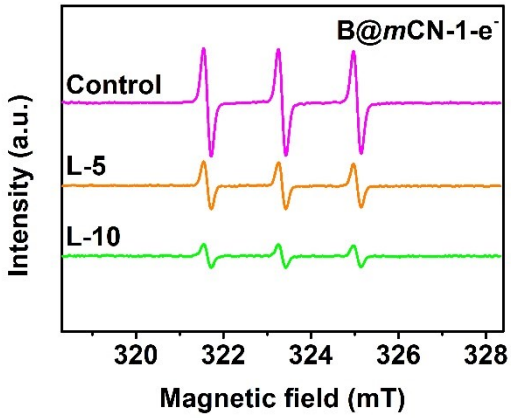

Fig. S7 TEMPO ESR spin-labelling for e^- of B@*m*CN-1.

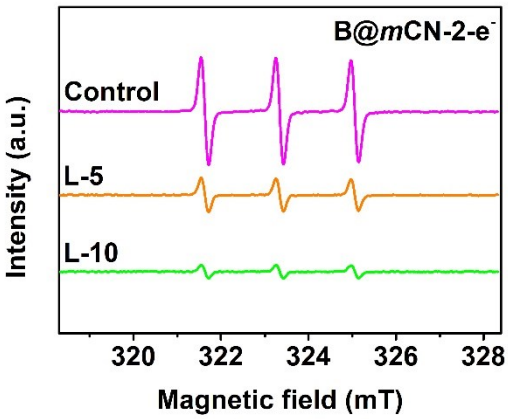

Fig. S8 TEMPO ESR spin-labelling for e^- of B@*m*CN-2.

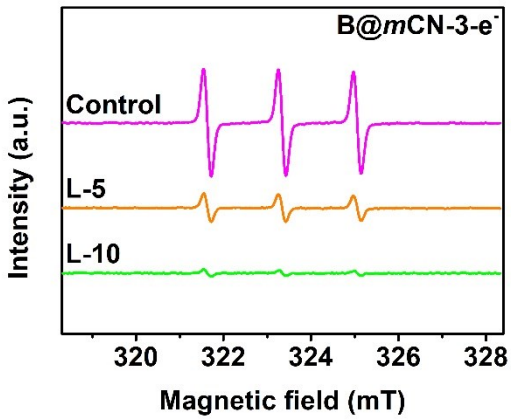

Fig. S9 TEMPO ESR spin-labelling for e^- of B@*m*CN-3.

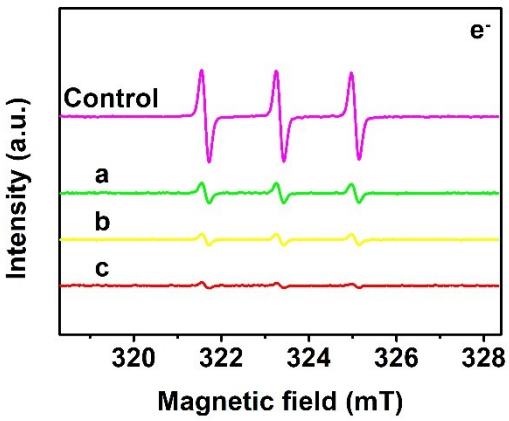

Fig. S10 TEMPO ESR spin-labelling for e^-, (a): B@*m*CN-1, (b): B@*m*CN-2, (c): B@*m*CN-3.

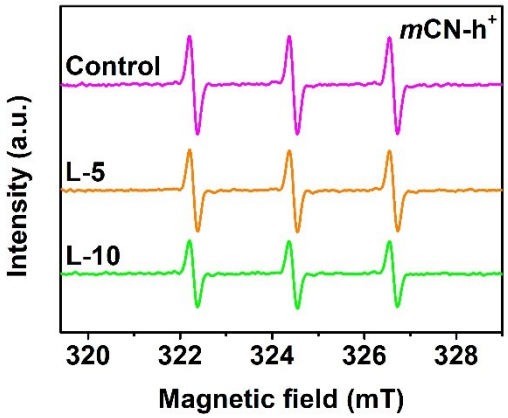

Fig. S11 TEMPO ESR spin-labelling for h^+ of *m*CN.

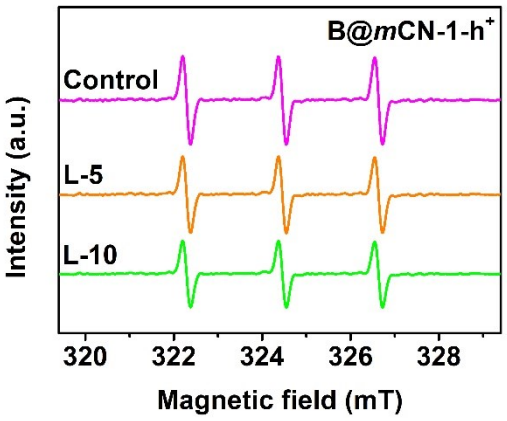

Fig. S12 TEMPO ESR spin-labelling for h^+ of B@*m*CN-1.

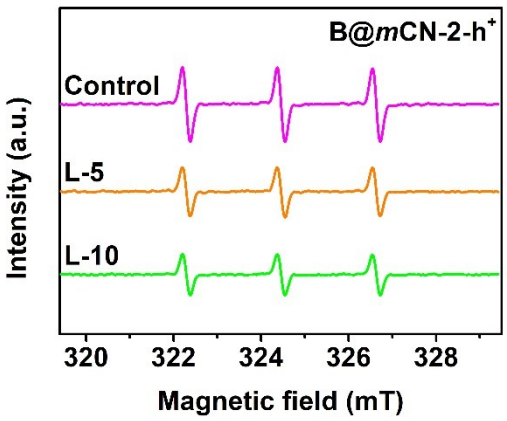

Fig. S13 TEMPO ESR spin-labelling for h^+ of B@*m*CN-2.

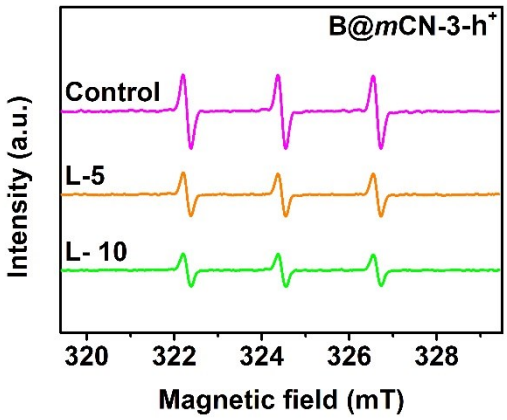

Fig. S14 TEMPO ESR spin-labelling for h^+ of B@*m*CN-3

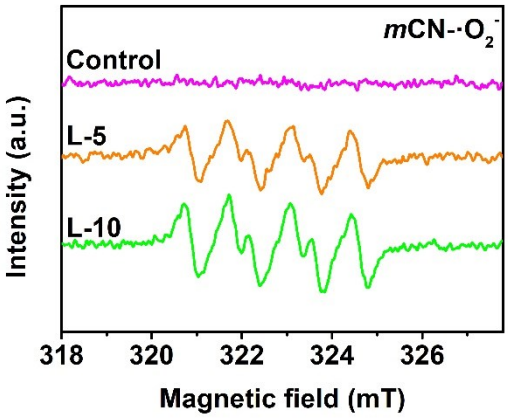

Fig. S15 DMPO ESR spin-labelling for $\cdot O_2^-$ of *m*CN.

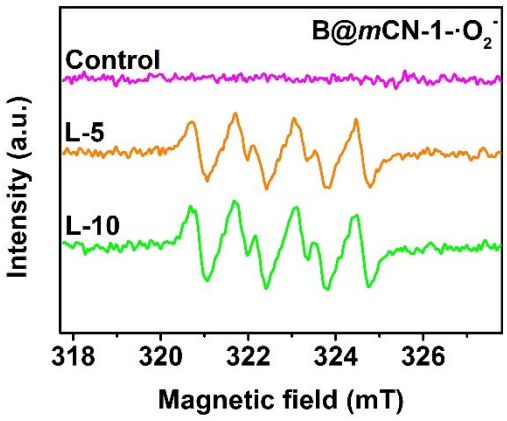

Fig. S16 DMPO ESR spin-labelling for $\cdot O_2^-$ of B@*m*CN-1.

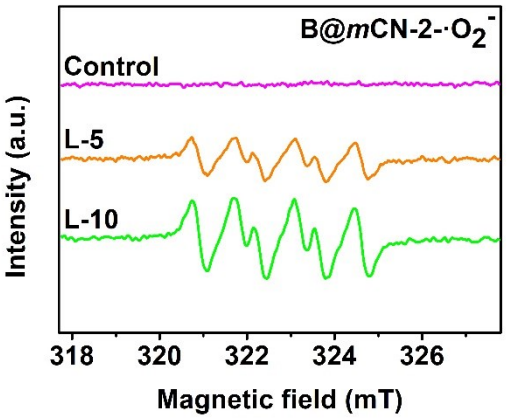

Fig. S17 DMPO ESR spin-labelling for $\cdot O_2^-$ of B@*m*CN-2.

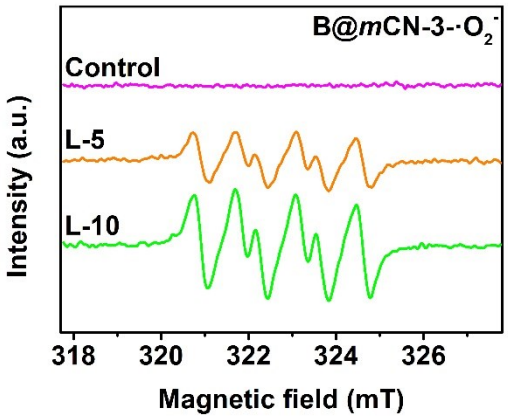

Fig. S18 DMPO ESR spin-labelling for $\cdot O_2^-$ of B@*m*CN-3.

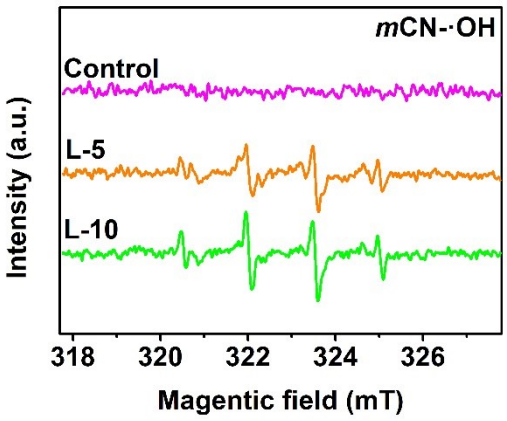

Fig. S19 DMPO ESR spin-labelling for ·OH of *m*CN.

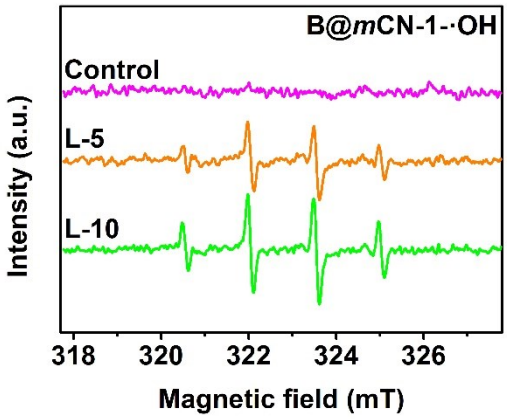

Fig. S20 DMPO ESR spin-labelling for ·OH of B@*m*CN-1.

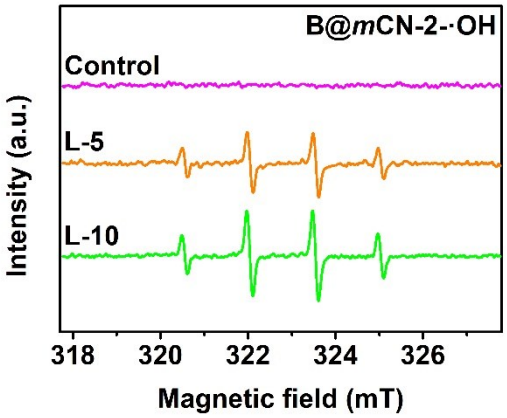

Fig. S21 DMPO ESR spin-labelling for ·OH of B@*m*CN-2.

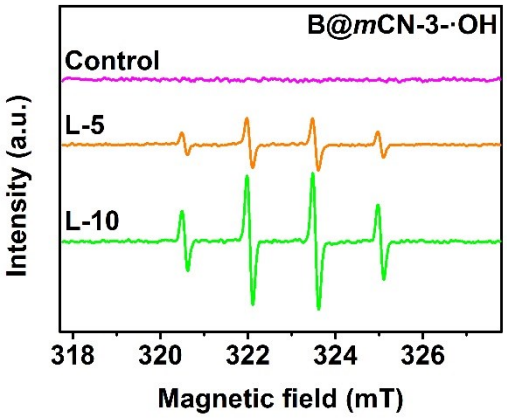

Fig. S22 DMPO ESR spin-labelling for ·OH of B@*m*CN-3.

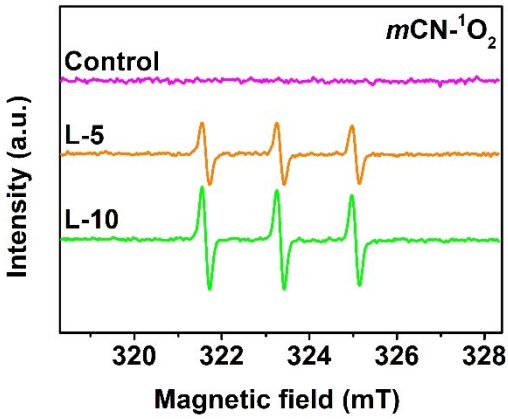

Fig. S23 TEMPONE ESR spin-labelling for $^1O_2$ of *m*CN.

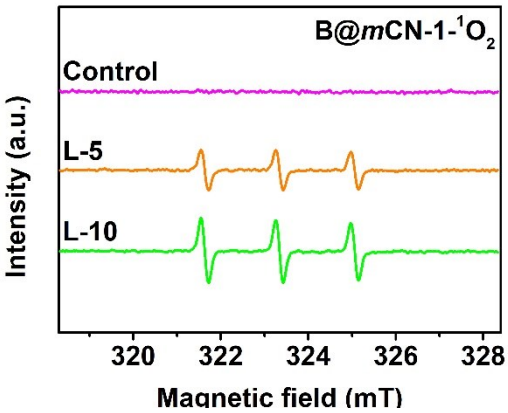

Fig. S24 TEMPONE ESR spin-labelling for $^1O_2$ of B@*m*CN-1.

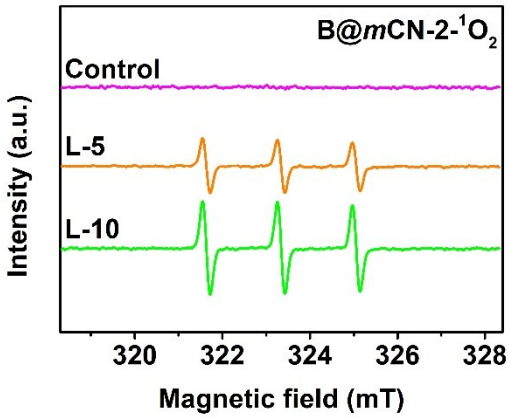

Fig. S25 TEMPONE ESR spin-labelling for $^1O_2$ of B@*m*CN-2.

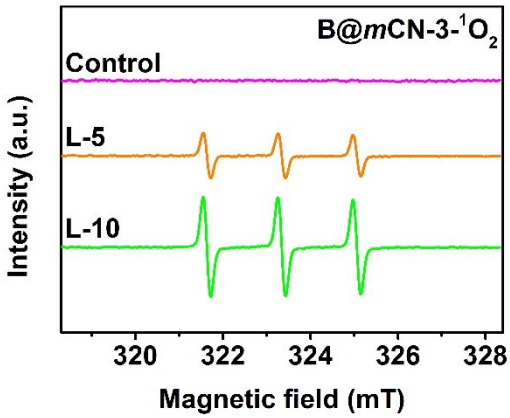

Fig. S26 TEMPONE ESR spin-labelling for $^1O_2$ of B@*m*CN-3.

Table S1 The O and B content of the catalysts

Entry	Samples	O (%) [a]	B (g/Kg) [b]
1	*m*CN	9.0	-
2	B@*m*CN-1	5.1	2.8
3	B@*m*CN-2	6.1	6.1
4	B@*m*CN-3	7.3	8.7

[a] The content of O element was detected by EA. [b] The content of B element was detected by ICP-MS.

Table S2 Various catalysts for the synthesis of lactic acid from glucose in their own appropriate reaction conditions

Entry	Catalyst	Glucose conversion	Lactic acid yield	Reaction conditions	Ref. [a]
1	B@*m*CN-3	＞ 99.0%	77.0%	60.0 °C, 1.5 h	this work
2	12-In/γ-Al_2O_3	＞ 99.0%	49.0%	180.0 °C, 10.0 h, N_2: 2.0 MPa	49
3	Sn-Beta-NH_2	＞ 99.0%	56.0%	190.0 °C, 2.0 h	50
4	Nb_2O_5 Nanorod	＞ 99.0%	39.0%	250.0 °C, 4.0 h	51
5	Zn-Sn-Beta zeolite	＞ 99.0%	56.0%	190.0 °C, 2.0 h	52
6	Sn-Beta zeolite	＞ 98.0%	67.1%	200.0 °C, 0.5 h, He: 4.0 MPa	53
7	$YNbO_4$-353	96.3%	19.6%	413.0 K, 5.0 h	54
8	Na_2SiO_3	-	30.0%	300.0 °C, 60.0 s	55

[a] The ref. have been listed in the main article.